Therapeutic targeting of KSP in preclinical models of high-risk neuroblastoma

Karin Hansson[1], Katarzyna Radke[1], Kristina Aaltonen[1], Jani Saarela[2], Adriana Mañas[1], Jonas Sjölund[1], Emma M. Smith[3], Sven Påhlman[1], Krister Wennerberg[2,4], David Gisselsson[5,6], Daniel Bexell[1*]

[1] Division of Translational Cancer Research, Department of Laboratory Medicine, Lund University, 223 81, Lund, Sweden

[2] Institute for Molecular Medicine Finland, University of Helsinki, 00290, Helsinki, Finland

[3] Division of Molecular Medicine and Gene Therapy, Lund Strategic Center for Stem Cell Biology, Lund University, 221 84, Lund, Sweden

[4] BRIC - Biotech Research & Innovation Centre, University of Copenhagen, 2200, Copenhagen, Denmark

[5] Division of Clinical Genetics, Department of Laboratory Medicine, Lund University, 221 85, Lund, Sweden

[6] Department of Pathology, Laboratory Medicine, Medical Services, University Hospital, 221 84, Lund, Sweden

* To whom correspondence should be addressed:

Daniel Bexell, MD, PhD

Division of Translational Cancer Research

Department of Laboratory Medicine

Lund University, Lund, Sweden

Phone: +46-46-2226423

E-mail: Daniel.bexell@med.lu.se

Abstract

Neuroblastoma is a childhood malignancy with often dismal prognosis; relapse is common despite intense treatment. Here, we used human tumor organoids representing multiple *MYCN*-amplified high-risk neuroblastomas to perform a high-throughput drug screen with approved or emerging oncology drugs. Tumor-selective effects were calculated using drug sensitivity scores. Several drugs with previously unreported anti-neuroblastoma effects were identified by stringent selection criteria. ARRY-520, an inhibitor of kinesin spindle protein (KSP), was among those causing reduced viability. High expression of the KSP-encoding gene *KIF11* was associated with poor outcome in neuroblastoma. Genome-scale loss-of-function screens in hundreds of human cancer cell lines across 22 tumor types revealed that *KIF11* is particularly important for neuroblastoma cell viability. KSP inhibition in neuroblastoma PDX cells resulted in the formation of abnormal monoastral spindles, mitotic arrest, upregulation of mitosis-associated genes, and apoptosis. In vivo, KSP inhibition caused regression of *MYCN*-amplified neuroblastoma PDX tumors. Furthermore, treatment of mice harboring orthotopic neuroblastoma PDX tumors resulted in increased survival. Our results suggested that KSP inhibition could be a promising treatment strategy in children with high-risk neuroblastoma.

One sentence summary: KSP inhibition results in cell death through mitotic arrest and causes regression of neuroblastoma PDX tumors in mice.

Introduction

Neuroblastoma is a pediatric malignancy of the sympathetic nervous system, with most primary tumors arising in the adrenal gland (*1*). Neuroblastoma patients are classified into risk groups (including high-, intermediate-, low-, and very low-risk) according to the international neuroblastoma risk group (INRG) classification system (*2*). Patients with high-risk tumors are treated aggressively with chemotherapy, surgery, radiotherapy, and autologous stem cell transplantation. However, high-risk tumors often relapse after completion of frontline therapy, and survivors suffer from lifelong severe side-effects (*3*). There is an urgent need to develop new treatment strategies for these children.

Neuroblastomas harbor relatively few somatic mutations at initial diagnosis, but relapsed tumors are enriched for genes predicted to activate oncogenic signaling pathways, such as the RAS-mitogen-activated protein kinase (MAPK) and the YAP-Hippo pathways (*4, 5*), paving the way for personalized treatment based on mutational profiles. However, neuroblastomas exhibit few recurrent and potentially druggable targets (*6*). In addition, high-risk neuroblastomas show substantial inter- and intratumoral heterogeneity (*7*), suggesting that any highly specific targeting may need to be complemented with a broader treatment strategy, for example cell-cycle inhibition, to completely eradicate tumors and minimize the risk of acquired resistance.

Cancer cell lines grown in 2D culture and conventional xenograft models have long been a mainstay of cancer research. To overcome some of their inherent limitations, 3D organoids and patient-derived xenograft (PDX) models have been developed and are increasingly being used. Recently, gastrointestinal cancer 3D patient-derived organoids were shown to effectively recapitulate clinical responses (*8*). Because addition of serum to tumor cell cultures results in

aberrant genotypes and the loss of drug-resistance mechanisms (*9*), serum-free culture conditions, which better recapitulate the biological characteristics of tumors (*10*), have also been applied when modeling cancer.

We previously established and characterized neuroblastoma orthotopic PDX models derived from high-risk tumors (*11*). These PDX models retain the genetic profiles, transcriptional signatures, protein markers, and invasive and metastatic phenotypes of their parent aggressive patient tumors (*12*). We also established PDX-derived human neuroblastoma organoids grown under serum-free conditions. The tumor organoids retain neuroblastoma-associated chromosomal aberrations and neuroblastoma protein markers, as well as tumorigenic and metastatic capacity upon re-implantation in vivo, making them particularly suitable for drug testing (*13*).

High-throughput drug screens have been a useful tool for identifying compounds effective in diverse tumor types (*14-16*). The few drug screens that have been performed for neuroblastoma (*17, 18*) identified a dequalinium analog, C-14 Linker (DECA-14), rapamycin (*17*), and polo-like kinase 1 (PLK1) inhibitors (*18*) as potential anti-neuroblastoma drugs. To identify previously untested effective therapies for high-risk neuroblastoma, here, we used neuroblastoma organoids and performed a high-throughput chemical drug screen. The drug library contains approved or emerging oncology drugs, which should facilitate rapid translation to clinical testing. We identified drugs previously known to target neuroblastoma as well as several other drugs with anti-neuroblastoma activity, including the highly selective inhibitor of kinesin spindle protein (KSP, also known as Eg5), ARRY-520 (filanesib) (*19-21*). Bioinformatic analysis of large data sets revealed that (i) the KSP-coding gene *KIF11* is associated with poor outcome in neuroblastoma, (ii) of 22 tumor types, neuroblastoma shows

highest *KIF11* gene dependency, and (iii) across 27 tumor types, neuroblastoma is among the most sensitive to KSP inhibition. Using the KSP inhibitor ARRY-520, a clinical-grade compound, and the related nonclinical-grade compound AR00423649 (AR649) (*22, 23*), we showed that inhibiting KSP in neuroblastoma results in formation of abnormal monoastral spindles, mitotic arrest, upregulation of genes associated with mitotic processes, and apoptosis in vitro, as well as complete tumor regression and increased survival time of mice harboring *MYCN*-amplified neuroblastoma PDX tumors.

Results

Establishment of a robust high-throughput drug screen

We previously established and characterized neuroblastoma orthotopic PDX models from high-risk tumors harboring chromosome arm 1p deletion, *MYCN* amplification, and 17q gain (*11*) (**Table 1**). From these tumors, we established free-floating neuroblastoma organoids grown under serum-free conditions (**Fig. 1A**) (*11, 13*). Here, we utilized the neuroblastoma organoids LU-NB-1, LU-NB-2, and LU-NB-3 for an untargeted high-throughput drug screen. The cell doubling times were 4.97 days for LU-NB-1, 4.74 days for LU-NB-2, and 2.92 days for LU-NB-3 (**fig. S1A and data file S1**).

The screen used a library of 525 approved or emerging investigational drugs (the FIMM oncology collection) belonging to different drug classes (**Fig. 1B and data file S2**). Tumor organoids were dissociated to single cells before seeding in 384-well plates pre-plated with drugs. The drug responses were analyzed using the CellTiter-Glo assay as a readout of cell viability. A titration experiment showed a linear relationship between viability and the number of cells in each well (**fig. S1B**). To assess the robustness of the assay, we calculated Z-factors for the difference in viability at each cell density using DMSO as a negative control (representing a compound that does not cause a reduction in viability) and the antiseptic benzethonium chloride as a positive control (representing a compound that causes total loss of cell viability). We found Z-factors > 0.5, the threshold for a robust difference, for all cell densities (**fig. S1C**).

In the main screen we used 5000 cells per well. Each set consisted of eight plates tested with six parameters (three PDX models and two different oxygen tensions). All 48 plates displayed

a Z-factor > 0.5 with a range of 0.59-0.86 and a mean Z-factor of 0.72 ± 0.06 (**Fig. 1C**), demonstrating excellent robustness of the assay.

Identification of drugs with anti-neuroblastoma effect

Each drug was tested at five concentrations in ten-fold dilutions, totaling 15,750 measurement points (525 drugs × 5 concentrations × 6 parameters) (**data file S3**). Concentrations producing a 50% reduction in viability (IC_{50}) and dose-response curves were calculated from the response at each concentration, and these data were used to calculate a drug sensitivity score (DSS) as previously described (*24*) (**fig. S1D**). A cutoff of 10 was applied for the DSS, above which drugs were considered effective (**Fig. 1D**).

Low oxygen tension is related to an aggressive neuroblastoma phenotype (*25*). To test the impact of oxygen tension on drug activity, the screen was performed at both 21% O_2 (normoxia) and 5% O_2 (physiological oxygen levels, physoxia). Overall, the correlation in drug response between 21 and 5% O_2 within each PDX model was high (R^2=0.93, 0.81, and 0.92; **Fig. 1E**). Although some individual drugs displayed different DSS at 21% and 5% O_2 within each PDX model, there were no drugs with differences at 21% and 5% O_2 across all PDX models (**fig. S2**).

To identify drugs with broad activity against high-risk neuroblastoma, we examined hits with a DSS ≥ 10 in all three PDX models at both 5% O_2 and 21% O_2 (**Fig. 2A**). This identified 96 drugs (**Fig. 2B**). We further selected those drugs with IC_{50} values < 1000 nM, which identified 87 common hits (**Fig. 2C**).

Identification of tumor-selective drugs

We aimed to identify drugs with tumor-selective activity and minimal off-target effects by comparing their effects on cell viability of PDX cells and healthy bone marrow-derived cells. Human bone-marrow derived cells from four healthy donors were used in a counter screen (mean Z-factor = 0.76 ± 0.035) (**fig. S3A).** A mean DSS was calculated for each drug within the control cells (**data file S3 and fig. S3B-C**). For each drug, we calculated a selective DSS (sDSS) with the formula: mean DSS (PDX cells) – mean DSS (control cells). With this formula, we identified 56 drugs with a sDSS ≥ 10 (**Fig. 2D**): 25 drugs were conventional chemotherapeutics, 21 were kinase inhibitors, 1 was an epigenetic modifier, 4 were apoptotic modulators, 3 were metabolic modifiers, and 2 were kinesin inhibitors (**Fig. 2E**). Many of these drugs have previously shown efficacy in neuroblastoma models. For example, inhibition of Aurora kinases (*26*), PLK1 (*18*), the phosphoinositide 3-kinase (PI3K)/mTOR pathway (*27*), the kinase CHK1 (*28*), the kinase WEE1 (*29*), and the E3 ubiquitin ligase MDM2 (*30*). However, some of the identified compounds have previously not been extensively tested in neuroblastoma (**Fig. 2F-G and fig. S3D**), among them the KSP inhibitor ARRY-520.

Association of KIF11 with poor survival in neuroblastoma

Analysis of the KSP-encoding gene *KIF11* in transcriptomic data from publicly available datasets (R2: Genomics Analysis and Visualization Platform) showed higher *KIF11* expression in neuroblastoma compared to that in adrenal gland or in various control tissues (**Fig. 3A**). In analyses of *KIF11* mRNA expression in 40 patient tumors, as well as in a range of cancer cell lines representing 34 tumor types (from the Cancer Cell Line Encyclopedia, CCLE), neuroblastoma was in the upper quartile when ranked according to *KIF11* expression (**Fig. 3B and fig. S4A**). Among neuroblastoma patient samples, *KIF11* showed higher expression in high-risk patient tumors compared to low-risk patient tumors (SEQC498 dataset) (**Fig. 3C**). In an independent dataset (Versteeg 88 dataset), *KIF11* expression was also significantly higher

stage 4 tumors compared to stage 1-3 (**Fig. 3D**), according to the INSS (International Neuroblastoma Staging System). High *KIF11* expression was associated with poor overall survival in both datasets (**Fig. 3E**). We found that *MYCN*-amplified tumors had higher *KIF11* expression compared to tumors without *MYCN* amplification (**fig. S4B)**. Furthermore, high *KIF11* expression was associated with poor survival in patients with non-*MYCN* amplified tumors (SEQ 498 dataset) (**fig. S4C**). There was no statistically significant association between *KIF11* expression and survival among patients with *MYCN*-amplified tumors (SEQ 498 dataset) (**fig. S4D**).

KIF11 gene dependency and drug response in neuroblastoma

Analysis of *KIF11* gene dependency in various tumor types was performed using CERES (*31*) and DEMETER2 (*32*) dependency score data from publicly available datasets. These scores are based on genome-wide viability screens in hundreds of cancer cell lines using CRISPR-Cas9 for CERES or RNAi for DEMETER2. The statistical tool in CERES controls for variations in sgRNA activity and copy number-specific effects when assessing genetic dependency in high-throughput knockout screens. Gene dependency estimates produced by the DEMETER2 algorithm have been corrected for off-target effects and batch effects, as well as fluctuation in screen quality. In both CERES and DEMETER2 scoring, the lower the score, the higher the dependency. Across 22 tumor types, neuroblastoma presented with the highest *KIF11* dependency using CERES ($p = 0.005$, two-sided unpaired t-test neuroblastoma versus all others; **Fig. 3F**). Similar results were obtained using DEMETER2 ($p = 0.0003$; **fig. S4E**). These findings suggested that, among this large panel of cancer cell lines, neuroblastoma is the most vulnerable tumor type to KSP antagonism. Both *MYCN* and non-*MYCN* amplified cell lines were included in the neuroblastoma panel in both the CERES and DEMETER2 datasets (**table S1**). Furthermore, analysis of data from the Genomics of Drug Sensitivity in Cancer (GDSC)

screening program (*33*), covering cell lines from 27 different tumor types, showed that neuroblastoma was among the most sensitive tumor types to ARRY-520 treatment (**Fig. 3G**) Again, both *MYCN* and non-*MYCN* amplified cell lines were included in the analysis (**table S2**). On the basis of these results, we continued with testing of KSP inhibition in neuroblastoma organoids and cell lines.

Inhibition of neuroblastoma cell viability by ARRY-520 and AR649

The effect of KSP inhibition in neuroblastoma was investigated using two highly specific KSP-inhibitors: ARRY-520, a clinical-grade compound (*19-21*), and the related nonclinical-grade compound AR00423649 (AR649) (*22, 23*). Both compounds contain a main 1,3,4-thiadiazole ring with a 5-phenyl group (**fig. S5A and B**), which is important for binding to the hydrophobic pocket of the KSP allosteric site (*34*). Both compounds have nanomolar IC_{50} values for KSP enzymatic activity in vitro and subnanomolar IC_{50} values for reducing viability of cells in culture (*21, 22*), and each exhibits a maximum tolerated dose in mg/kg in mice (*20, 23*), indicating that these are compounds with properties consistent with clinical application (**fig. S5C**). We found that the three PDX cell models as well as the conventional neuroblastoma cell lines IMR-32, SK-N-FI, SK-N-BE(2)c, and SK-N-SH (representing both *MYCN*-amplified and non-*MYCN*–amplified tumors) displayed KSP protein expression (**fig. S6A-B**). Using the CellTiter-Glo assay, we confirmed that both inhibitors decreased viability of neuroblastoma PDX cells in a dose-dependent manner at subnanomolar concentrations (**Fig. 4A-B and data file S1**). Compared to LU-NB-1 and LU-NB-2, LU-NB-3 showed higher sensitivity to each inhibitor. The inhibitors were also effective in reducing viability of the conventional neuroblastoma cell lines (**fig. S7A and data file S1**).

G2/M cell cycle arrest caused by KSP inhibition

KSP is important for the formation of spindle bipolarity during mitosis (*35*). Cell cycle analysis showed that 24 h-treatment of PDX cells and conventional neuroblastoma cell lines with AR649 or ARRY-520 increased the fraction of cells in G2/M phase (**Fig. 4C and fig. S7B-D)**, indicating that they had been blocked from completing mitosis. There was also an increase of cells in the sub-G1 phase, representing dead cells, particularly in the LU-NB-3 model (**Fig. 4C and fig. S7C**). We performed immunofluorescence staining of β-tubulin and γ-tubulin with LU-NB-2 cells. We found that AR649 treatment (24 h) induced the formation of abnormal monoastral spindles, whereas control cells formed bipolar mitotic spindles (**Fig. 4D**). Quantification of LU-NB-2 cells in mitosis, identified by β-tubulin staining and morphology, showed a significant increase in mitotic cells in the treated samples ($p = 0.002$, two-sided unpaired t-test, **Fig. 4E-F**), consistent with the cell cycle analysis that revealed a G2/M phase arrest under the same conditions (**Fig. 4C**).

Upregulation of cell cycle-associated genes by KSP inhibition

To further elucidate the effects of KSP inhibition in neuroblastoma, we performed RNA sequencing (RNA-seq) on LU-NB-2 PDX cells treated with ARRY-520 (0.5 nM, 24h). We identified 19 differentially expressed genes between treated and untreated cells (ANOVA, $p < 0.01$, FDR correction). Treated samples showed upregulation of genes related to cell cycle progression, such as *KIF20A*, *CENPA*, and *AURKA* (**Fig. 4G**). Gene ontology analysis showed that genes significantly upregulated in treated cells were enriched in mitosis-related processes, including chromatid segregation, spindle organization, and nuclear division (**Fig. 4H and data file S4**).

Induction of apoptosis in neuroblastoma by KSP inhibition

Although KSP inhibition decreased neuroblastoma cell viability, this does not necessarily indicate cell death occurred. To establish whether cells were dying, we treated neuroblastoma organoids with AR649 or ARRY-520 (0.5 nM, 72h). There was clear morphological evidence of cell death (**Fig. 5A and fig. S8A**). To quantify the effect of the inhibitors on neuroblastoma cell death, we performed annexin V and propidium iodide (PI) flow cytometry. Treatment increased the proportion of dead cells at nanomolar concentrations and, consistent with the results of the screen and the cell cycle analysis, LU-NB-3 was more sensitive than LU-NB-1 and LU-NB-2, showing nearly complete loss of viable cells in response to AR649 (**Fig. 5B and data file S1**) and < 10% live cells in response to ARRY-520 (**fig. S8B-C and data file S1**). The EC_{50} values for the death-inducing effect of AR649 were 0.11 nM for LU-NB-3, 0.16 nM for LU-NB-2, and 0.17 nM LU-NB-1. KSP inhibition also caused death of conventional *MYCN*-amplified and non-*MYCN* amplified neuroblastoma cell lines (**fig. S8B-C**).

To explore the mechanism of cell death, we analyzed AR649-treated LU-NB-2 cells using the caspase-3/7 substrate NucView405. Flow cytometry at 24, 48, and 72 h of treatment showed caspase activation, particularly at 72 h (**Fig. 5C**). The timing of caspase activation corresponded with that of an increased fraction of PI-positive cells (**Fig. 5C**). Similar effects were seen in PDX cells and conventional neuroblastoma cell lines treated for 72 h with ARRY-520 (**fig. S8D**). Thus, both AR649 and ARRY-520 effectively induced neuroblastoma cell death at nanomolar concentrations.

Anti-neuroblastoma effects of KSP inhibitors SB-743921 and ispinesib

To evaluate different KSP inhibition treatment strategies in neuroblastoma, we also treated neuroblastoma PDX cells with KSP inhibitors SB-743921 and ispinesib (also known as SB-715992). These compounds are small molecules with related structures, but their structures

differ from those of than ARRY-520 and AR649 (**fig. S9A-B**). Both SB-743921 and ispinesib showed dose-dependent reductions in neuroblastoma cell viability (**fig. S9C-D and data file S1**) and caused G2/M cell cycle arrest (**fig. S9E-F**). This indicated that structurally diverse compounds that inhibit KSP have anti-neuroblastoma effects.

Mitotic arrest induced by short-term KSP inhibition in vivo

To investigate the effect of KSP inhibition in vivo, mice carrying PDX tumors were treated with AR649. LU-NB-3 PDX cells were injected subcutaneously into nude mice. Mice were individually allocated to control or treatment groups when the tumor size had reached at least 500 mm^3 (**fig. S10A**). Each mouse was treated intraperitoneally (i.p.) with either AR649 at a dose of 5 mg/kg or saline at day 1, 5 and 9 (**Fig. 6A**). There was no statistically significant difference in the growth of tumors in treated mice compared to that in the untreated controls ($p = 0.08$, two-sided unpaired t-test) (**Fig. 6B and data file S1**). Immunohistochemistry revealed the presence of neuroblastoma markers neural cell adhesion molecule (NCAM, also known as CD56), synaptophysin, and chromogranin A in PDX tumors from both AR649-treated and saline-treated mice (**fig. S10B**). Hematoxylin and eosin (H&E) staining showed that all tumors from control mice had an undifferentiated tumor morphology (small blue round cells with scant cytoplasm), whereas the tumors from the AR649-treated mice displayed morphological signs of neuroblastoma differentiation including a marked increase in neurofibrillary stroma (**Fig. 6C**). Immunohistochemistry showed no difference in the number of proliferative ($Ki67^+$) cells between tumors from treated and control mice ($p = 0.73$, two-sided unpaired t-test). However, AR649 treatment increased a subpopulation of mitotic $Ki67^+$ cells, identified by their condensed chromosomes ($p = 0.003$, two-sided unpaired t-test) (**Fig. 6D-F**), which was confirmed morphologically (**Fig. 6G-H**). Compared to mitotic cells in the control samples, AR649 increased the fraction of cells in the prophase of mitosis ($p<0.0001$, Mann-Whitney U

test) (**Fig. 6I and data file S1**). There was no statistically significant increase in apoptotic cells as assessed by TUNEL staining after this short treatment (**fig. S10C-D**). Taken together, short-term AR649 treatment caused morphological signs of neuroblastoma differentiation and cell cycle arrest in the early phases of mitosis in vivo.

Regression of neuroblastoma PDX tumors in vivo by long-term KSP inhibition

We investigated the effect of long-term KSP inhibition on neuroblastoma PDX growth. LU-NB-3 PDX cells were injected subcutaneously into nude mice. Mice were individually allocated to control or treatment groups when the tumor size reached at least 150 mm^3 (**fig. S11A**). Mice were treated i.p. with either AR649 at a dose of 1.5 mg/kg or saline twice weekly for six weeks (**Fig. 7A**). Mice were monitored for weight loss (**fig. S11B**) and tumor growth (**fig. S11C**). Treatment with AR649 decreased PDX tumor growth ($p = 0.03$ after three treatment injections, two-sided unpaired t-test; **Fig. 7B** and **fig. S11C**), and treatment induced a complete response (CR) in 6/8 mice (**Fig. 7C**). AR649 also prolonged survival time of PDX mice: Four of the 8 treated mice survived the entire study period of 120 days; 3 mice had a median survival of 99 days (range 81-116). One treated mouse was euthanized on day 25 due to ≥ 15% weight loss. The controls had a median survival of 32 days (range 18-39 days) (**Fig. 7D**). Thus, these results show that KSP inhibition has the potential to cause regression of high-risk *MYCN*-amplified neuroblastoma PDX tumors.

Increased survival in orthotopic neuroblastoma PDX models by KSP inhibition

We next tested clinical-grade ARRY-520 in orthotopic neuroblastoma PDX models. Luciferase-expressing LU-NB-1 PDX cells were injected orthotopically into the adrenal gland of immunodeficient NSG mice. Mice were individually allocated to control or treatment groups when tumors were detected using bioluminescence imaging (**fig. S12A**). Tumor-bearing mice

were treated i.p. with ARRY-520 at a dose of 12.5 mg/kg or saline twice weekly for nine weeks (**Fig. 7E**). Mice were observed for weight loss and signs of toxicity (**fig. S12B)**. Tumor growth was monitored using bioluminescence imaging in vivo (**Fig. 7F** and **fig. S12C**). Treatment with ARRY-520 prolonged survival time of orthotopic LU-NB-1 PDX mice, with a median survival of 34 days (range 27-57) for control mice and 57 days (range 38-62) for treated mice ($p = 0.004$, log-rank test). Two treated mice were euthanized due to ≥ 15% weight loss (on days 38 and 45) (**Fig. 7G**).

We also tested ARRY-520 in orthotopic LU-NB-2 PDX tumors, established from a treatment-resistant relapse. Luciferase-expressing cells were injected into the adrenal gland of nude mice and mice were individually allocated to control or treatment groups when tumors were detected using bioluminescence imaging (**fig. S13A**). Mice were treated i.p. with ARRY-520 at a dose of 12.5 mg/kg or saline twice weekly for nine weeks (**Fig. 7H**). All mice tolerated the treatment well (**fig. S13B**). In vivo bioluminescence imaging revealed markedly decreased orthotopic tumor growth following ARRY-520 treatment ($p = 0.002$ at day 28, two-sided unpaired t-test; **Fig. 7I** and **fig. S13C-E**). ARRY-520 significantly increased the survival time of the PDX mice from 55 days (range 42-62) in control mice to 83 days (range 63-112) in treated mice ($p = 0.003$, log-rank test) (**Fig. 7J**).

In vivo anti-neuroblastoma effects without weight loss in response to ARRY-520

To shed light on the therapeutic window of ARRY-520, we evaluated the effect of lower dosing (10 mg/kg) in vivo. LU-NB-3 PDX cells were injected subcutaneously into nude mice and mice were individually allocated to control or treatment groups when the tumors reached at least 150 mm^3 (**fig. S14A**). Mice were treated i.p. with ARRY-520 (10 mg/kg twice weekly for 25 days) (**fig. S14A**). All mice tolerated the treatment without weight loss (**fig. S14B**). All mice were

euthanized on day 25. This treatment paradigm significantly decreased PDX tumor growth compared to growth in control mice ($p = 0.03$ at day 11, two-sided unpaired t-test) (**fig. S14C-D**). Thus, our results from multiple PDX models showed that KSP inhibition decreases tumor growth and increases survival time of mice harboring *MYCN*-amplified high-risk neuroblastoma.

Discussion

High-risk neuroblastoma remains a lethal disease in many cases despite intensive cytotoxic therapeutic regimens; novel therapeutic strategies are urgently needed. The low number of recurrent potentially druggable targets in many neuroblastomas, high intertumoral heterogeneity, remarkable levels of spatial intratumoral heterogeneity, and significant temporal clonal evolution (*4, 5, 7, 12, 36-38*) suggest that strategies that target common mechanisms across neuroblastoma populations may be valuable to completely eradicate tumors and prevent the emergence of acquired resistance. Here, we performed a high-throughput drug screen using a library of approved or emerging oncology compounds tested against *MYCN*-amplified human neuroblastoma PDX cells. We identified several drug candidates with efficacy against high-risk neuroblastoma. In addition to identifying drugs with previously known preclinical effects in neuroblastoma (inhibitors targeting Aurora A, PLK1, WEE1, CHK1, MDM2, and the PI3K/mTOR pathway), we also identified agents not extensively investigated in neuroblastoma, including the kinesin (KIF) inhibitors GSK923295 and ARRY-520, pevonedistat, daporinad, AVN944, selinexor, BAY 87-2243, UCN-01, rigosertib, KX2-391, and CUDC-101. We selected the KSP inhibitor ARRY-520 because of the association of *KIF11* expression with clinical outcome, gene dependency data, as well as a consistent drug response in multiple neuroblastoma models.

KSP is a motor protein that binds to microtubules to support the formation of bipolar spindles, which are essential for chromosome segregation during cell division. KSP inhibitors specifically target mitotic cells. This contrasts with traditional microtubule inhibitors, including those used in current neuroblastoma therapy, which also affect non-mitotic cells (*19, 39*). Additionally, KSP is not present in mature neurons, so KSP inhibition may not induce neurotoxicity, a common side-effect of conventional microtubule inhibitors (*40*). The first-

generation KSP inhibitor ispinesib has anti-tumor effects in conventional xenograft models of pediatric cancers, although only low-to-intermediate activity was observed in neuroblastoma (*41, 42*). The KSP inhibitor ARRY-520 used in the present study has shown efficacy in preclinical models of mainly hematological malignancies (*19, 20*), and ARRY-520 is currently being tested in a clinical trial against multiple myeloma (NCT02384083). Notably, our findings that (i) *KIF11* expression is associated with poor outcome in neuroblastoma, (ii) neuroblastoma shows the highest *KIF11* gene dependency across multiple tumor types, (iii) neuroblastoma is among the most sensitive tumors to ARRY-520 across 27 tumor types, and (iv) treatment with AR649 resulted in complete response in 6 out of 8 neuroblastoma PDX mice, strengthen the case for the use of KSP inhibition in neuroblastoma.

As with all preclinical drug testing studies, it is worth reflecting on the translational relevance and potential limitations of our study. One important aspect is that cultured cancer cells and in vivo models often have much faster tumor cell doubling times (a higher fraction of mitotic tumor cells) compared to the cancer cells in patient tumors (*43*). Care must therefore be taken when drawing clinical conclusions from results of the effects of anti-mitotic drugs in relatively fast-growing culture and in vivo models. Despite this limitation, there was still a significant effect of ARRY-520 in the slowest growing PDX model in vivo (LU-NB-2 PDX, derived from a treatment-resistant relapse), indicating that tumor growth rate is not the only factor dictating response to KSP inhibition. Similarly, toxicity testing of bone marrow cells in vitro (as performed in the counter screen) might not necessarily reflect bone marrow toxicity in vivo. Regarding the mode of action, we cannot exclude the possibility that the anti-neuroblastoma activity may be due to additional mechanisms other than KSP inhibition. Another limitation is that our study was performed with mice, which could have a different pharmacokinetic profile

for the drug than would pediatric patients. It is unknown whether similar drug concentrations can be obtained in pediatric patients as in mice.

We noted, based on mouse weight, that severely immunodeficient NSG mice seemed more sensitive to ARRY-520 compared to nude mice. Based on previous clinical studies, reversible neutropenia, stomatitis, and mucositis can be dose-limiting factors when targeting KSP (*44*). Assessment of the biomarker Alpha 1-Acid Glycoprotein (AAG), an acute-phase reactant protein, could be one approach to select patients who would benefit most from ARRY-520 treatment, because high concentrations of AAG can alter the pharmacokinetics of ARRY-520 (*45*).

Future studies should address the mechanisms of cell death following KSP inhibition. Anti-mitotic drugs usually cause mitotic arrest, but apoptotic responses are variable in different tumors (*46*). This diversity could be due to differences in survival signaling pathways in different tumor cells. For instance, in multiple myeloma cells treated with ARRY-520, destabilization of the anti-apoptotic protein myeloid cell leukemia (Mcl-1) is important for the onset of apoptosis following mitotic arrest (*47*).

In conclusion, by performing a high-throughput drug screen of approved or emerging drugs using neuroblastoma PDX cells, we identified several anti-neuroblastoma drugs. We show powerful effects of KSP inhibition in multiple high-risk neuroblastoma PDX models in vitro and in vivo. Notably, we observed complete tumor regression in one high-risk *MYCN*-amplified PDX model in mice. Mechanistically, KSP inhibitors caused neuroblastoma cells to undergo mitotic arrest with monoastral spindles and upregulation of cell cycle-related genes, followed by apoptosis. Experimental and clinical data suggest that KSP inhibition is most effective as a

combination therapy (*48*). Potential treatment combination strategies include co-targeting of KIF15 (*49*), Aurora A, and microtubule regulating proteins MCAK and KIF18B (*50*). Substituting or adding KSP inhibitors to current treatment regimens could increase the efficacy and prolong the survival of patients with high-risk neuroblastoma.

Materials and Methods

Study design

The aim of this study was to identify potential neuroblastoma treatments. We performed a high-throughput drug screen using neuroblastoma PDX cells to identify drugs with tumor-selective activity against neuroblastoma. The high-throughput screen was performed once for each condition (PDX model and oxygen tension) and each 384-well plate contained both positive and negative controls. Among the top ranking drugs, we selected the KSP inhibitor ARRY-520 for further testing, because bioinformatics analyses indicated high *KIF11* expression and gene dependency in neuroblastoma. We investigated the effects of KSP inhibition in vitro using tumor organoid models and conventional neuroblastoma cell lines. For in vitro experiments, two or three biological replicates were performed (reported for each experiment). For in vivo studies, 10 mice per group were injected with PDX cells and depending on the tumor engraftment, 4-10 mice were randomly allocated to treatment or control groups. Sample size was determined on the basis of previous experimental evidence. Investigators were not blinded to the experiments. We did not exclude any tumor-carrying mice from the studies. Mice were euthanized if they showed weight loss ≥ 15% or if tumor volume reached 1800 mm^3.

Tumor organoids

Neuroblastoma PDX-derived cells LU-NB-1, LU-NB-2, and LU-NB-3 were cultured in serum-free medium as previously described (*11, 13*). Briefly, cells were grown as tumor organoids in Dulbecco's Modified Eagle's Medium (DMEM) and GlutaMAX F-12 in a 3:1 ratio, supplemented with 1% penicillin/streptomycin, 2% B27 without vitamin A, 40 ng/ml fibroblast growth factor, and 20 ng/ml epidermal growth factor. The cells were regularly verified by single nucleotide polymorphism (SNP) analysis and screened for mycoplasma. A Whitley H35 Hypoxystation (Don Whitley Scientific) was used to generate 5% O_2.

Neuroblastoma cell lines

The human neuroblastoma cell lines SK-N-BE(2)c, SK-N-SH, SK-N-FI, and IMR-32 were purchased from ATCC. Cells were cultured in minimal essential medium (MEM; SK-N-BE(2)c and SK-N-SH) or RPMI (SK-N-FI and IMR-32) supplemented with 10% fetal bovine serum (FBS) and 1% penicillin/streptomycin. The cells were regularly verified by SNP analysis and screened for mycoplasma.

High-throughput drug screen

The FIMM oncology drug set of 525 drugs (F04B) was used. Each drug was plated at five concentrations in 10-fold dilutions in 384-well plates. The drugs were dissolved in 10 µl medium and incubated for 30 minutes before adding the cells. The neuroblastoma organoids were dissociated to single cells, and 5000 cells were subsequently added to each well for a total volume of 25 µl. The plates were incubated for 72 h in 21% O_2 or 5% O_2 at 37°C and 5% CO_2. After 72 h, cell viability was measured using the CellTiter-Glo luminescent assay (G7571, Promega) according to the manufacturer's instructions. Luminescence was measured using a Synergy2 plate reader (Biotek) and the Gen5 software (Biotek). The raw data were analyzed using the Breeze pipeline (https://breeze.fimm.fi) for curve fitting and to obtain quality control and drug response parameters, such as Z', DSS, sDSS, IC_{50}, and EC_{50} (*51*).

Assay validation and drug selection

Each plate in the screen included both negative controls for compounds that do not cause a reduction in viability (DMSO) and positive controls for compounds that cause a reduction in viability (100 µmol/L benzethonium chloride). These were used to calculate a Z-factor as a measure of the robustness of the screen. Dose-response curves and DSS were generated as

previously described (*52*). The dose-response curves were fitted based on four parameters: top and bottom asymptote, the IC_{50}, and slope at IC_{50}. The DSS is defined as the area under the dose response curve, compared to the total graph area, above a 10% threshold. The response of different drugs was compared using the DSS, where a DSS ≥ 10 was considered an effective response. The IC_{50} was also used to select drugs with activity at low drug concentrations (IC_{50} < 1000 nM). For identification of tumor-selective drugs, we utilized bone marrow-derived cells from healthy individuals. Briefly, bone marrow aspirates were collected after signed informed consent from each patient (permit numbers 239/13/03/00/2010, 303/13/03/01/2011, Helsinki University Hospital ethics committee). The counter screen was performed on four healthy bone marrow samples and the average luminescence values from the CellTiter-Glo assay were used to calculate the DSS for control cells. The formula DSS (PDX cells) – DSS (control cells) was used to calculate an sDSS for the neuroblastoma PDX cells. Drugs with sDSS ≥ 10 were selected for further investigation.

Bioinformatics analyses

Publicly available datasets were obtained from and analyzed with R2: Genomics Analysis and Visualization Platform (http://r2.amc.nl). The datasets SEQC498 and Versteeg88, containing 498 and 88 neuroblastomas, respectively, were used for analysis of *KIF11* gene expression. The expression in neuroblastoma (Versteeg88) was compared to various normal tissue (Roth 504) and normal tissue from the adrenal gland (Various 13), as well as the largest available datasets from other cancer diagnoses across platforms hs, u133p2, MAS5.0. Gene probe set 204444_a is used for all datasets. Within neuroblastoma, expression of *KIF11* was compared between high- and low-risk tumors (SEQC498) or between INSS stages (Versteeg88). Statistical analyses were performed using two-sided unpaired t-tests. For analysis of overall survival between high and low *KIF11* expression in Kaplan-Meier curves, the median was used

as a cut-off and statistical significance was calculated using the log-rank test. Expression of *KIF11* in cell lines was extracted from the Cancer Cell Line Encyclopedia (CCLE, https://portals.broadinstitute.org/ccle). CERES (*31*) and DEMETER2 (*32*) dependency scores were obtained from DepMap portal (https://depmap.org/portal/) at the Broad Institute by downloading the CRISPR dataset (DepMap Public 19Q3, Dataset doi:10.6084/m9.figshare.9201770.v1.) and the combined RNAi dataset (DEMETER2 Data v5). Tumor types with data from less than five cell lines were excluded from subsequent analyses. Publicly available data on IC_{50} values of ARRY-520 was obtained from the Genomics of Drug Sensitivity in Cancer (GDSC) database (*33*) (https://www.cancerrxgene.org).

Drug formulations

KSP inhibitors AR649 and ARRY-520 were provided by Array Biopharma (Boulder, CO, USA). For in vitro experiments, the compounds were dissolved in DMSO, diluted in medium, and used in a concentration range of 0.01 to 10 nM. For in vivo purposes, inhibitors were dissolved in saline (0.9% NaCl). AR649 was diluted to 1 mg/ml and administered at 1.5-5 mg/kg by intraperitoneal injection; ARRY-520 was diluted to 1.25 mg/ml and administered at 10 – 12.5 mg/kg by intraperitoneal injection. Ispinesib and SB-743921 (Selleckchem) were dissolved in DMSO, diluted in medium, and used in a concentration range of 0.01 to 10 nM.

Cell viability assay

Cell viability was measured using CellTiter-Glo (Promega Corp.). Single cells were seeded and treated in triplicates in opaque 96-well plates in a total volume of 100 µl. The neuroblastoma cell lines SK-N-BE(2)c, SK-N-SH, SK-N-FI, and IMR-32 were incubated for 24 hours before treatment to allow attachment to the plate. PDX cells were treated directly after seeding. After

72 h treatment, 50 µl CellTiter-Glo reagent was added to each well, and the luminescence was measured using a Synergy2 plate reader (Biotek) and Gen5 software (Biotek).

Cell doubling times

Cells were seeded and quantified using trypan blue every 24 hours for 8 days. Growth curves were obtained using the equation Y = Y0*exp(k*X); where Y0 is the Y value when X is 0, k is the rate constant in 1/days, and X is time in days. Doubling times were computed using the equation (duration *log(2))/(log(final conc) - log(initial conc)).

Western blot

Cells were lysed in RIPA buffer, supplemented with complete protease inhibitor (Roche) and phosSTOP (Roche). Proteins were separated using SDS-PAGE gels and transferred to Hybond-C-Extra nitrocellulose membranes (Bio-Rad). Antibodies used: KSP/Eg5 (#14404, Cell Signaling, 1:1000) and SDHA (Ab14715, Abcam, 1:4000) as a loading control.

Cell cycle analysis

Single cells were treated for 24 h and then fixed in ice cold 70% ethanol and kept at -20°C. Upon analysis, they were washed in PBS and incubated on ice for 45 min in Vindelöv solution [3.5 µmol/L Tris-HCl (pH 7.6), 10 mmol/L NaCl, 50 µg/mL propidium iodide, 20 µg/mL RNase, 0.1% v/v NP40]. Samples were run on a FACSVerse flow cytometer (BD Biosciences), and the data were analyzed using FlowJo software.

Immunofluorescence

LU-NB-2 cells were seeded on glass slides pre-coated with 10 µg/ml laminin (LN521-05, Biolamina) for adherent growth. Cells were allowed to attach for 24 h and were then treated for

24 h. Cells were fixed in 4% paraformaldehyde, permeabilized with 0.5% Triton-X, and blocked using 5% goat serum. Staining of microtubules was performed using β-tubulin antibody diluted 1:100 (ab15568, Abcam), and centrosomes were stained using γ-tubulin antibody diluted 1:100 (ab11316, Abcam). Secondary fluorescent antibodies were diluted 1:1000 (A11008 and A11032, Invitrogen), and cell nuclei were visualized with DAPI staining 1:3000 (D3571, Invitrogen).

RNA sequencing

LU-NB-2 cells were treated with 0.5 nM ARRY-520 or vehicle control for 24 h. RNA extraction was performed using the AllPrep DNA/RNA Mini Kit (Qiagen), and 500 ng of total RNA was used for input to library preparation. The mRNA library preparation was performed with TruSeq Stranded mRNA Library Prep (Illumina) on the King Fisher FLEX system (Thermo Fisher Scientific). NextSeq 500 (Illumina) was used for sequencing using the NextSeq 500/550 High Output v2.5 kit (Illumina). Reads were aligned to the human GRCh38 (ENSEMBL database) reference genome sequence and the annotation (GTF) from release 94 using HISAT2 software. Gene level assembly and quantification were performed using StringTie, and raw counts were normalized using DESeq2. All data were uploaded to the R2: Genomic Analysis and Visualization Platform (http://r2.amc.nl) under the name PDX Neuroblastoma KSPi-in-vitro_20190416 - Aaltonen - 16 - deseq2 - ensh38e94. Library preparation, mRNA sequencing, and data normalization were performed by the Center for Translational Genomics (CTG), Lund University and Clinical Genomics Lund, SciLifeLab. All RNA-seq analyses were performed on the R2 platform.

Treatment of tumor organoids

PDX cells were cultured for 72 h to form tumor organoids before treatment. Tumor organoids were treated with DMSO or 0.5 nM of AR649 or ARRY-520. Treatment response was evaluated by morphological analysis of the organoids.

Cell death analysis

Cell death was evaluated by Annexin V and PI staining. Apoptosis was analyzed using Nucview405 (Biotium). Treated cells (72 h) were dissociated to single cells, and the same amount of suspension was obtained from each sample. Samples were stained with 5% APC annexin V and 2% PI for cell death analysis and with 0.5% Nucview405 together with 2% PI for analysis of apoptosis. The samples were incubated for 15 min and then run on a FACSVerse flow cytometer (BD Biosciences). Data were analyzed using FlowJo software.

Generation of viral vectors

A third-generation lentiviral vector expressing eGFP and luciferase under the control of the PGK-promoter was generated. The vector was generated by subcloning an internal ribosomal entry site (IRES) followed by the coding sequence of *Photinus pyralis* (firefly) luciferase immediately downstream of the constitutively active phosphoglycerate kinase (PGK) promoter and eGFP in a third-generation lentiviral vector. The IRES and luciferase fragments were obtained by PCR using the following primers: ires XhoI s, 5'-AGCATTCTCGAGTAGCTAGCTGAGGC CGCTCAC; ires SalI MluI as, 5'-GTATGCGTCGACTTCTAATCGAACGCGTGGTGGAA TTCTGCAGATATCC; Luc MluI s, 5'-AGACTCACGCGTATGGAAGACGCCAAAAACA TAAAG; Luc SalI as, 5'-GTATGCGTCGACTTACAATTTGGACTTTCCGCCCTTC. The IRES fragment was cloned into a *SalI* site located a few base pairs downstream of the eGFP stop codon. In a second subcloning step, luciferase was cloned downstream of the IRES using the restriction sites

MulI/SalI. The final lentiviral vector construct was verified by sequencing. The neuroblastoma PDX cells were transduced using MOI5, and transduction was verified by investigating eGFP expression using flow cytometry.

Animal experiments

NMRI-Nude mice were purchased from Taconic and NSG mice from Charles River Laboratories. All procedures were conducted according to the guidelines from the regional Ethics Committee for Animal Research (ethical permit no. M11-15 and 19012-19).

For the AR649 short-term LU-NB-3 PDX in vivo study, LU-NB-3 PDX cells (2×10^6) were suspended in a 100 µl mixture of medium and Matrigel (2:1) and injected subcutaneously into the flanks of female nude mice. Tumor size was measured using a digital caliper and calculated with the formula $V=(\pi ls^2)/6$ mm^3 (where l is the long side and s is the short side). Each mouse was individually allocated to control or treatment groups when its tumor had reached at least 500 mm^3, with a mean size of 920 mm^3 among all mice. Mice were treated by intraperitoneal injection with 5 mg/kg AR649 (n=5) or saline (n=4) at day 1, 5, and 9 and were euthanized 5-7 hours after the last treatment. Tumor sections were evaluated by immunohistochemistry using blinded analyses.

For the AR649 long-term LU-NB-3 PDX in vivo study, LU-NB-3 PDX cells (2×10^6) were suspended in a 100 µl mixture of medium and Matrigel (2:1) and injected subcutaneously into the flanks of female nude mice. Tumor size was measured as above. Each mouse was individually allocated to control or treatment groups when its tumor had reached at least 150 mm^3 (mean size 220 mm^3 for all mice). Mice were treated by intraperitoneal injection with either AR649 (initial bolus dose of 5 mg/kg and subsequently treatment twice weekly with 1.5

mg/kg for six weeks, n=8) or with saline (n=7). Mice were monitored for weight loss and other signs of toxicity. Mice were euthanized when tumors reached 1800 mm^3 or had weight loss ≥ 15% of initial weight. The study was finalized 120 days after start of treatment.

For the ARRY-520 LU-NB-1 orthotopic PDX in vivo study, luciferase-expressing LU-NB-1 PDX cells (2×10^6) were suspended in a 30 µl mixture of medium and Matrigel (2:1) and injected orthotopically into the adrenal glands of male NSG mice, as previously described (*11*). This study was performed in severely immunodeficient NSG mice due to higher tumor engraftment rate of the LU-NB-1 PDX model in this mouse strain. Orthotopic tumors were monitored using bioluminescence imaging in vivo, and treatment was started individually for each mouse when tumors were detected. Mice were treated by intraperitoneal injection with 12.5 mg/kg ARRY-520 (n=8) or saline (n=8) twice weekly for a maximum of nine weeks. Treatment was paused if mice displayed weight loss ≥ 10 %. Mice were euthanized when they showed general signs or symptoms due to tumor burden or at weight loss ≥ 15% of initial weight.

For the ARRY-520 LU-NB-2 orthotopic PDX in vivo study, luciferase-expressing LU-NB-2 PDX cells (2×10^6) were injected orthotopically in the adrenal glands of female nude mice, as described previously (*11*). Orthotopic tumors were monitored using bioluminescence imaging and treatment started individually for each mouse when tumors were detected. Mice were treated by intraperitoneal injection with 12.5 mg/kg ARRY-520 (n=5) or saline (n=4) twice weekly for nine weeks. Mice were euthanized according to the criteria described above.

For the ARRY-520 LU-NB-3 PDX in vivo study, LU-NB-3 PDX cells (2×10^6) were suspended in a 100 µl mixture of medium and Matrigel (2:1) and injected subcutaneously into

the flanks of female nude mice. Tumor size was measured with calipers as described for the other subcutaneous tumor experiments. Each mouse was individually allocated to control or treatment groups when tumors had reached at least 150 mm^3 (mean size 242 mm^3 for all mice). Mice were treated by intraperitoneal injection with either ARRY-520 (10 mg/kg, n=5 per group) or with saline (n=5) twice weekly for 25 days. Mice were monitored for weight loss and other signs of toxicity. All mice were euthanized 25 days after start of treatment.

Bioluminescence imaging

In vivo bioluminescence imaging was performed using the IVIS Spectrum CT (Perkin Elmer). Mice were anaesthetized by 2 – 3% isoflurane inhalation and injected with 150 mg/kg of D-luciferin (Perkin Elmer) subcutaneously. Mice were placed onto a warmed stage inside the camera box with continuous exposure to isoflurane. Imaging exposure time was set to 120 seconds, and sequential images were taken every 5 min for 20 min. Images were analyzed using Living Image 4.5.5 software, where regions of interests (ROIs) were drawn and quantified as photons/second.

Immunohistochemistry

Tumors were fixed in 4% formalin and embedded in paraffin. The tumors were cut in 4-µm sections and stained using AutostainerPlus (Dako). Antibodies used: neural cell adhesion molecule (NCAM/CD56) (1:50, NCL-L-CD56-501, Leica Biosystems), chromogranin A (1:500, M0869, Dako), and synaptophysin (1:100, M7315, Dako). Hematoxylin & eosin (HistoLab Products AB) was used for assessment of histopathology, and the TUNEL assay (ab206386, Abcam) was used to assess cell death. Quantification of staining was performed using CellProfiler-3.1.8. For quantification of cells in different mitotic phases in H&E stained sections, 50 mitotic cells from six tumor sections were manually calculated and then divided

into prophase, metaphase, or anaphase based on the morphology. The researcher performing the quantification was blinded to the sample.

Statistical analyses

Statistical analyses were performed in GraphPad Prism 8.1 (GraphPad) or IBM SPSS Statistics 25 (IBM). For microarray data, the publicly available datasets SEQC498 and Versteeg88 containing 498 and 88 neuroblastomas, respectively, were used (obtained from and analyzed using R2: Genomics Analysis and Visualization Platform; http://r2.amc.nl). Comparison of drug responses under 21% and 5% O_2 conditions were performed using linear regression analysis. The two-sided unpaired t-test was used to analyze differences between groups. Statistical significance for Kaplan-Meier survival analyses was calculated using the log-rank test. To analyze the difference in distribution of mitotic phases between samples, the two-tailed Mann-Whitney U-test was used. Data from RNA sequencing was analyzed using one-way analysis of variance (ANOVA) with a 0.01 false discovery rate (FDR) correction for multiple testing. Gene ontology analysis was performed with 2×2 contingency table analysis (chi-square) with continuity correction.

Supplementary Materials

Figure S1. Establishment of a high-throughput chemical drug screen.

Figure S2. Drug response at 5% O_2 and 21% O_2.

Figure S3. Human bone marrow-derived control cells in the counter screen

Figure S4. KIF11 mRNA expression and gene dependency

Figure S5. Biochemical properties of ARRY-520 and AR649

Figure S6. KSP abundance in neuroblastoma cells

Figure S7. KSP inhibition causes neuroblastoma cell cycle arrest

Figure S8. ARRY-520 causes neuroblastoma cell death

Figure S9. Anti-neuroblastoma effects of KSP inhibitors SB-743921 and ispinesib

Figure S10. Immunohistochemistry following AR649 treatment in vivo

Figure S11. Characteristics of AR649–treated LU-NB-3 PDX model in vivo

Figure S12. Characteristics of ARRY-520–treated LU-NB-1 orthotopic PDX model in vivo

Figure S13. Characteristics of ARRY-520–treated LU-NB-2 orthotopic PDX model in vivo

Figure S14. Characteristics of ARRY-520–treated LU-NB-3 PDX model in vivo

Table S1. KIF11 gene dependency analysis of neuroblastoma cell lines.

Table S2. ARRY-520 sensitivity in neuroblastoma cell lines.

Data file S1. Original data for figures presenting mean values.

Data file S2. Complete list of the 525 drugs (the FIMM oncology set) included in the high-throughput screen.

Data file S3. Complete data from the high-throughput drug screen.

Data file S4. Complete Gene Ontology list based on upregulated genes following ARRY-520 treatment of LU-NB-2 PDX cells.

References and notes

1. N. K. Cheung, M. A. Dyer, Neuroblastoma: developmental biology, cancer genomics and immunotherapy. *Nat Rev Cancer* **13**, 397-411 (2013).
2. S. L. Cohn *et al.*, The International Neuroblastoma Risk Group (INRG) classification system: an INRG Task Force report. *J Clin Oncol* **27**, 289-297 (2009).
3. J. M. Maris, Recent advances in neuroblastoma. *The New England journal of medicine* **362**, 2202-2211 (2010).
4. A. Schramm *et al.*, Mutational dynamics between primary and relapse neuroblastomas. *Nat Genet* **47**, 872-877 (2015).

5. T. F. Eleveld *et al.*, Relapsed neuroblastomas show frequent RAS-MAPK pathway mutations. *Nat Genet* **47**, 864-871 (2015).

6. D. T. W. Jones *et al.*, Molecular characteristics and therapeutic vulnerabilities across paediatric solid tumours. *Nat Rev Cancer* **19**, 420-438 (2019).

7. J. Karlsson *et al.*, Four evolutionary trajectories underlie genetic intratumoral variation in childhood cancer. *Nat Genet* **50**, 944-950 (2018).

8. G. Vlachogiannis *et al.*, Patient-derived organoids model treatment response of metastatic gastrointestinal cancers. *Science* **359**, 920-926 (2018).

9. J. P. Gillet *et al.*, Redefining the relevance of established cancer cell lines to the study of mechanisms of clinical anti-cancer drug resistance. *Proc Natl Acad Sci U S A* **108**, 18708-18713 (2011).

10. J. Lee *et al.*, Tumor stem cells derived from glioblastomas cultured in bFGF and EGF more closely mirror the phenotype and genotype of primary tumors than do serum-cultured cell lines. *Cancer Cell* **9**, 391-403 (2006).

11. N. Braekeveldt *et al.*, Neuroblastoma patient-derived orthotopic xenografts retain metastatic patterns and geno- and phenotypes of patient tumours. *International journal of cancer* **136**, E252-261 (2015).

12. N. Braekeveldt *et al.*, Patient-derived xenograft models reveal intratumor heterogeneity and temporal stability in neuroblastoma. *Cancer Res* **78** (20), 5958-5969 (2018).

13. C. U. Persson *et al.*, Neuroblastoma patient-derived xenograft cells cultured in stem-cell promoting medium retain tumorigenic and metastatic capacities but differentiate in serum. *Sci Rep* **7**, 10274 (2017).

14. P. B. Gupta *et al.*, Identification of selective inhibitors of cancer stem cells by high-throughput screening. *Cell* **138**, 645-659 (2009).

15. J. M. Atkinson *et al.*, An integrated in vitro and in vivo high-throughput screen identifies treatment leads for ependymoma. *Cancer Cell* **20**, 384-399 (2011).

16. Y. Pei *et al.*, HDAC and PI3K Antagonists Cooperate to Inhibit Growth of MYC-Driven Medulloblastoma. *Cancer Cell* **29**, 311-323 (2016).

17. K. M. Smith *et al.*, Selective targeting of neuroblastoma tumour-initiating cells by compounds identified in stem cell-based small molecule screens. *EMBO Mol Med* **2**, 371-384 (2010).

18. N. Grinshtein *et al.*, Small molecule kinase inhibitor screen identifies polo-like kinase 1 as a target for neuroblastoma tumor-initiating cells. *Cancer Res* **71**, 1385-1395 (2011).

19. B. Z. Carter *et al.*, Inhibition of KSP by ARRY-520 induces cell cycle block and cell death via the mitochondrial pathway in AML cells. *Leukemia* **23**, 1755-1762 (2009).

20. R. Woessner *et al.*, ARRY-520, a novel KSP inhibitor with potent activity in hematological and taxane-resistant tumor models. *Anticancer Res* **29**, 4373-4380 (2009).

21. C. Lemieux *et al.*, ARRY-520, a novel, highly selective KSP inhibitor with potent anti-proliferative activity. *Cancer Research* **67**, 5590-5590 (2007).

22. M. R. Miglarese *et al.*, ARRY-649, a member of a novel class of Eg5 kinesin inhibitors. *Journal of Clinical Oncology* **24**, 13045-13045 (2006).

23. E. M. Wallace *et al.*, ARRY-649: A potent and efficacious kinesin spindle protein inhibitor. *4th International Symposium on Targeted Anti-Cancer Therapies (Abstract)*, (2006).

24. B. Yadav *et al.*, Quantitative scoring of differential drug sensitivity for individually optimized anticancer therapies. *Sci Rep* **4**, 5193 (2014).

25. C. Wigerup, S. Pahlman, D. Bexell, Therapeutic targeting of hypoxia and hypoxia-inducible factors in cancer. *Pharmacology & therapeutics* **164**, 152-169 (2016).

26. W. C. Gustafson *et al.*, Drugging MYCN through an allosteric transition in Aurora kinase A. *Cancer Cell* **26**, 414-427 (2014).

27. L. Chesler *et al.*, Inhibition of phosphatidylinositol 3-kinase destabilizes Mycn protein and blocks malignant progression in neuroblastoma. *Cancer Res* **66**, 8139-8146 (2006).

28. C. D. Lowery *et al.*, The Checkpoint Kinase 1 Inhibitor Prexasertib Induces Regression of Preclinical Models of Human Neuroblastoma. *Clin Cancer Res* **23**, 4354-4363 (2017).

29. E. Stewart *et al.*, Orthotopic patient-derived xenografts of paediatric solid tumours. *Nature* **549**, 96-100 (2017).

30. T. Van Maerken *et al.*, Small-molecule MDM2 antagonists as a new therapy concept for neuroblastoma. *Cancer Res* **66**, 9646-9655 (2006).

31. R. M. Meyers *et al.*, Computational correction of copy number effect improves specificity of CRISPR-Cas9 essentiality screens in cancer cells. *Nat Genet* **49**, 1779-1784 (2017).

32. J. M. McFarland *et al.*, Improved estimation of cancer dependencies from large-scale RNAi screens using model-based normalization and data integration. *Nature Communications* **9**, 4610 (2018).

33. W. Yang *et al.*, Genomics of Drug Sensitivity in Cancer (GDSC): a resource for therapeutic biomarker discovery in cancer cells. *Nucleic Acids Research* **41**, D955-D961 (2012).

34. S. K. Talapatra *et al.*, Crystal structure of the Eg5 - K858 complex and implications for structure-based design of thiadiazole-containing inhibitors. *Eur J Med Chem* **156**, 641-651 (2018).

35. A. Blangy *et al.*, Phosphorylation by p34cdc2 regulates spindle association of human Eg5, a kinesin-related motor essential for bipolar spindle formation in vivo. *Cell* **83**, 1159-1169 (1995).

36. L. H. Mengelbier *et al.*, Intratumoral genome diversity parallels progression and predicts outcome in pediatric cancer. *Nat Commun* **6**, 6125 (2015).

37. V. Boeva *et al.*, Heterogeneity of neuroblastoma cell identity defined by transcriptional circuitries. *Nat Genet* **49**, 1408-1413 (2017).

38. T. van Groningen *et al.*, Neuroblastoma is composed of two super-enhancer-associated differentiation states. *Nature Genetics* **49**, 1261 (2017).

39. W. Tao *et al.*, Induction of apoptosis by an inhibitor of the mitotic kinesin KSP requires both activation of the spindle assembly checkpoint and mitotic slippage. *Cancer Cell* **8**, 49-59 (2005).

40. M. R. Miglarese, R. O. Carlson, Development of new cancer therapeutic agents targeting mitosis. *Expert Opin Investig Drugs* **15**, 1411-1425 (2006).

41. H. Carol *et al.*, Initial testing (stage 1) of the kinesin spindle protein inhibitor ispinesib by the pediatric preclinical testing program. *Pediatr Blood Cancer* **53**, 1255-1263 (2009).

42. C. C. Mills, E. A. Kolb, V. B. Sampson, Recent Advances of Cell-Cycle Inhibitor Therapies for Pediatric Cancer. *Cancer Res* **77**, 6489-6498 (2017).

43. E. Komlodi-Pasztor, D. L. Sackett, A. T. Fojo, Inhibitors targeting mitosis: tales of how great drugs against a promising target were brought down by a flawed rationale. *Clin Cancer Res* **18**, 51-63 (2012).

44. P. M. LoRusso *et al.*, First-in-human phase 1 study of filanesib (ARRY-520), a kinesin spindle protein inhibitor, in patients with advanced solid tumors. *Invest New Drugs* **33**, 440-449 (2015).

45. B. Tunquist *et al.*, Identification of Alpha 1-Acid Glycoprotein (AAG) As a Potential Patient Selection Biomarker for Improved Clinical Activity of the Novel KSP Inhibitor ARRY-520 in Relapsed and Refractory Multiple Myeloma (MM). *Blood* **120**, 1868-1868 (2012).

46. J. Shi, J. D. Orth, T. Mitchison, Cell type variation in responses to antimitotic drugs that target microtubules and kinesin-5. *Cancer Res* **68**, 3269-3276 (2008).

47. B. J. Tunquist, R. D. Woessner, D. H. Walker, Mcl-1 stability determines mitotic cell fate of human multiple myeloma tumor cells treated with the kinesin spindle protein inhibitor ARRY-520. *Mol Cancer Ther* **9**, 2046-2056 (2010).

48. G. Chandrasekaran, P. Tatrai, F. Gergely, Hitting the brakes: targeting microtubule motors in cancer. *British journal of cancer* **113**, 693-698 (2015).

49. B. Milic, A. Chakraborty, K. Han, M. C. Bassik, S. M. Block, KIF15 nanomechanics and kinesin inhibitors, with implications for cancer chemotherapeutics. *Proceedings of the National Academy of Sciences of the United States of America* **115**, E4613-e4622 (2018).

50. R. van Heesbeen *et al.*, Aurora A, MCAK, and Kif18b promote Eg5-independent spindle formation. *Chromosoma* **126**, 473-486 (2017).

51. S. Potdar *et al.*, Breeze: an integrated quality control and data analysis application for high-throughput drug screening. *Bioinformatics* **36**, 3602-3604 (2020).

52. T. Pemovska *et al.*, Individualized systems medicine strategy to tailor treatments for patients with chemorefractory acute myeloid leukemia. *Cancer discovery* **3**, 1416-1429 (2013).

53. S. C. Jost, L. Collins, S. Travers, D. Piwnica-Worms, J. R. Garbow, Measuring brain tumor growth: combined bioluminescence imaging-magnetic resonance imaging strategy. *Mol Imaging* **8**, 245-253 (2009).

54. A. A. Khalil *et al.*, The Influence of Hypoxia and pH on Bioluminescence Imaging of Luciferase-Transfected Tumor Cells and Xenografts. *Int J Mol Imaging* **2013**, 287697 (2013).

55. T. N. T. Le *et al.*, Characterization of an Orthotopic Rat Model of Glioblastoma Using Multiparametric Magnetic Resonance Imaging and Bioluminescence Imaging. *Tomography* **4**, 55-65 (2018).

Acknowledgments

We thank Javanshir Esfandyari for excellent technical help. Lund University and Medicon village are gratefully acknowledged for providing IVIS-CT experimental resources. We thank Array Biopharma for providing ARRY-520 and AR649. We thank the Center for Translational Genomics, Lund University for providing sequencing services. Editorial services were provided by Nancy R. Gough (BioSerendipity, LLC, Elkridge, MD).

Funding

This work was supported by grants from the Swedish Cancer Society (D.B., S.P.), Swedish Childhood Cancer Foundation (D.B., S.P.), the Swedish Research Council (D.B.), the Strategic Cancer Research Program BioCARE (D.B.), the Medical Faculty of Lund University (D.B.), Crafoord Foundation (D.B.), Jeanssons stiftelser (D.B.), Mary Béves Stiftelse för Barncancerforskning (D.B.), Ollie och Elof Ericssons stiftelser (D.B.), Berth von Kantzows stiftelse (D.B.), The Royal Physiographic Society in Lund, (D.B., K.H.) Per-Eric and Ulla Schyberg foundation (D.B.), Åke Wiberg Foundation (D.B.), Magnus Bergvall Foundation (D.B.), Märta Winklers stiftelse (D.B.), Gyllenstiernska Krapperupsstiftelsen (D.B.), Region Skåne and Skåne University Hospital (ALF-medel) (D.B.). The FIMM High Throughput

Biomedicine Unit is financially supported by the University of Helsinki (HiLife) and Biocenter Finland.

Author contributions

K.H., K.W., D.G., and D.B. designed the research; K.H., K.R., A.M., E.S., and D.B performed experiments; K.H., K.R., K.A., J.Sa., J. Sj., S.P., K.W., D.G., and D.B. analyzed data; K.H., and D.B. wrote the manuscript; D.B. supervised the research. All authors read and approved the manuscript.

Competing interests

The authors declare that they have no competing interests.

Data and materials availability

RNA sequencing data generated during these studies have been deposited to the R2: Genomic Analysis and Visualization Platform (http://r2.amc.nl) under the name PDX Neuroblastoma KSPi-in-vitro_20190416 - Aaltonen - 16 - deseq2 - ensh38e94. All other data associated with this study are present in the paper or Supplementary Materials.

Table 1. Overview of neuroblastoma PDX models. INSS – International Neuroblastoma Staging System; AG – adrenal gland; UD – undifferentiated; PD – poorly differentiated. *MYCN* amp, *MYCN* amplification; SNP – single nucleotide polymorphism

Patient	**Cells**	**Age**	**Sample type**	**Chemotherapy**	**INSS stage**	**Histology**	**SNP profile**
1	LU-NB-1	1y4m	Primary (AG)	No	IV	UD	*MYCN* amp, 1p-, 17q+

2	LU-NB-2	2y2m	Metastasis	Yes, sample from a treatment-resistant relapse.	IV	UD	*MYCN* amp, 1p-, 17q+
3	LU-NB-3	2y9m	Primary (AG)	No	III	PD	*MYCN* amp, 1p-, 17q+

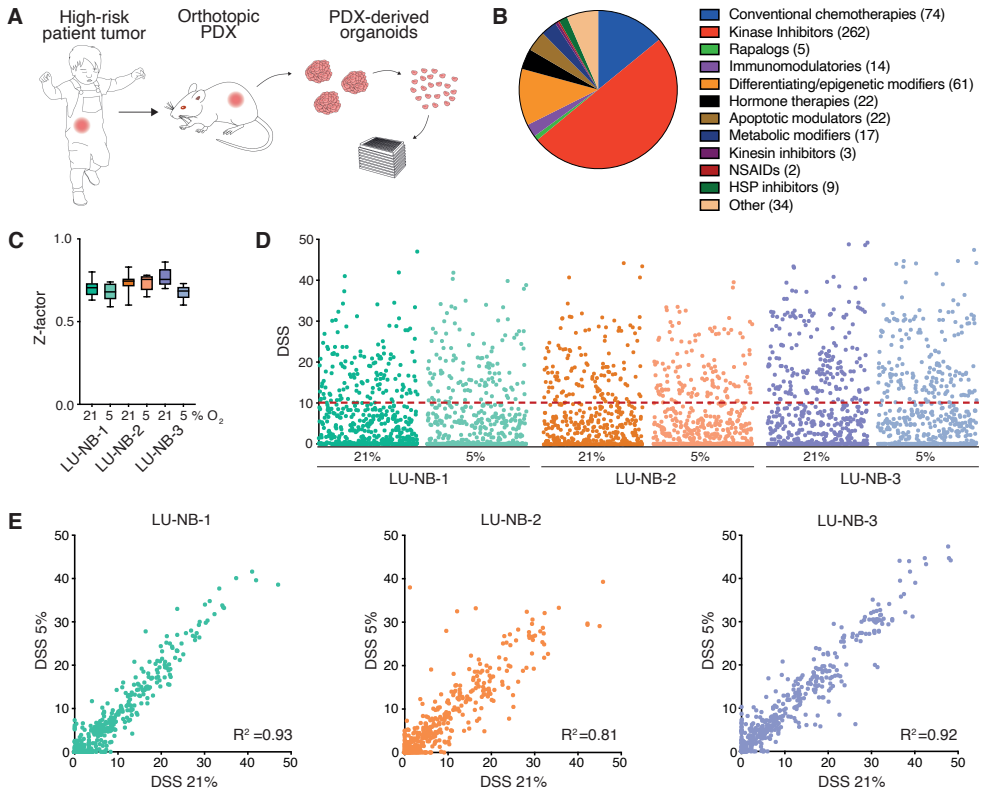

Figure 1. A high-throughput drug screen to identify drugs targeting high-risk neuroblastoma. **(A)** Establishment of cells for screen. Free-floating 3D tumor organoids were established from *MYCN*-amplified neuroblastoma orthotopic PDX models (LU-NB-1, LU-NB-2, LU-NB-3) and cultured under serum-free conditions. Tumor organoids were dissociated to single cells and seeded in 384-well plates. **(B)** Categories of compounds in the chemical library (the FIMM oncology set) used for the screen. The numbers in parentheses show the number of compounds within each category. Experiments were performed at five concentrations per drug in 384-well plates. **(C)** The Z-factors of cell viability for each plate of cells from the PDX

models (cells from one model per 384-well plate). The boxes show the 25th to 75th percentiles, lines show the median and whiskers represent minimum and maximum Z-factors for each plate of cells cultured at the indicated oxygen concentrations. **(D)** The DSS for each drug in the three models (LU-NB-1, LU-NB-2, and LU-NB-3) at two oxygen concentrations (21% O_2 and 5% O_2). **(E)** Comparison of the DSSs at 21% O_2 and 5% O_2 for each PDX model. DSS, drug sensitivity score; PDX, patient-derived xenograft; FIMM, Institute for Molecular Medicine Finland.

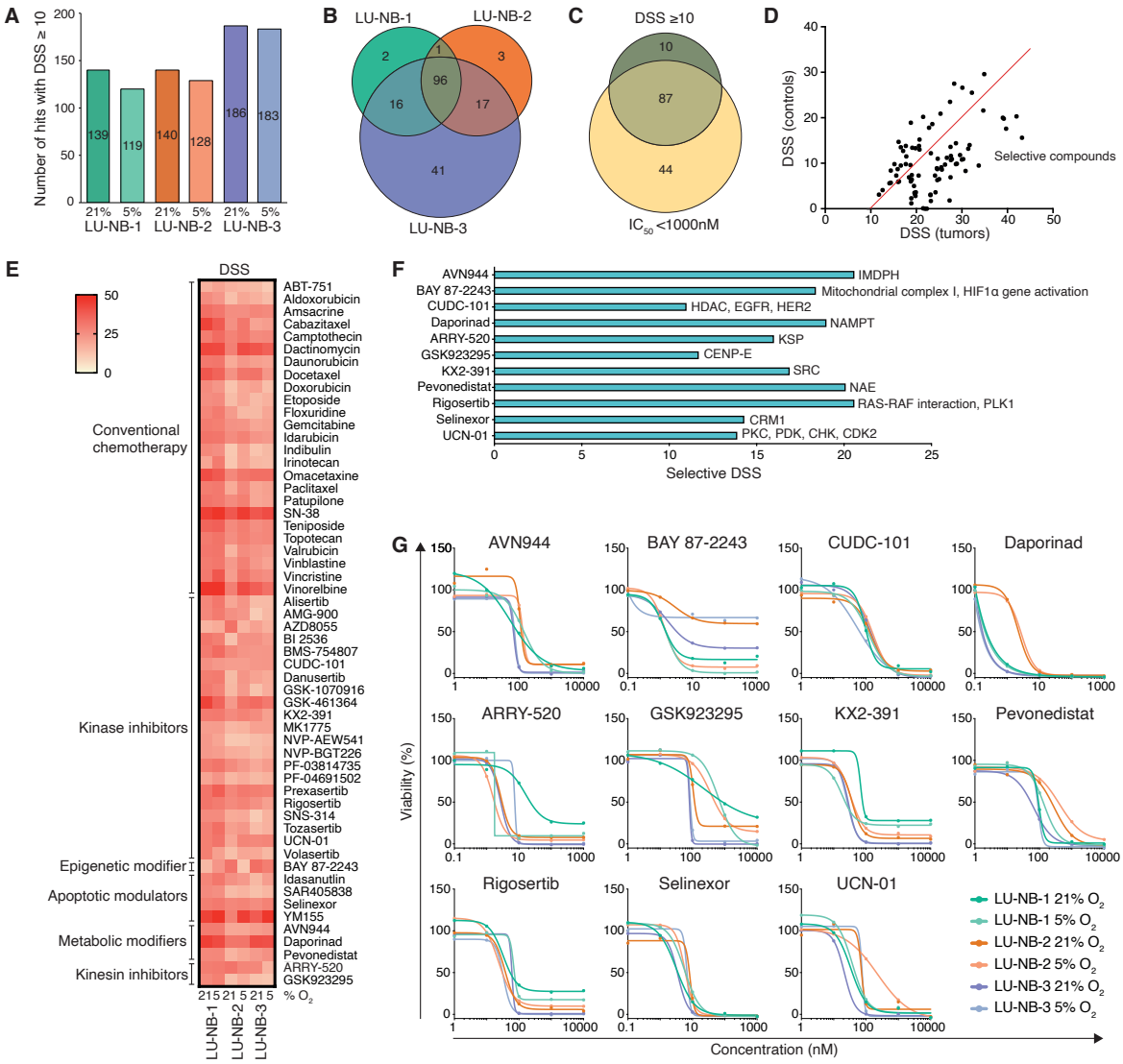

Figure 2. Identification of tumor-selective drugs. **(A)** The number of drugs with a drug sensitivity score (DSS) ≥10. **(B)** Venn diagram of identified drugs with DSS ≥10 in three PDX models at 5% and 21% O_2. **(C)** Venn diagram showing number of drugs with DSS ≥10 and IC_{50}

<1000 nM in all three PDX models and at both oxygen tensions. **(D)** Identification of drugs with a difference in DSS between neuroblastoma PDX cells and healthy control bone marrow-derived cells. Only those drugs with a DSS ≥10 in tumors were included. Compound scoring to the right of the red line exhibit tumor selectivity. **(E)** The DSS of drugs with a selective DSS ≥10 in all PDX models at two oxygen concentrations (n = 56 drugs). **(F)** DSS for selected drugs previously not extensively tested in neuroblastoma. The drug names (y axis) and their respective targets (after bar) are shown. **(G)** Dose-response curves for the effect of 11 tumor-selective drugs on cell viability. DSS, drug sensitivity score; PDX, patient-derived xenograft; IMDPH, Inosine-5′-monophosphate dehydrogenase; HIF1α, hypoxia-inducible factor 1α; HDAC, histone deacetylase, EGFR, epidermal growth factor receptor; HER2, human epidermal growth factor receptor 2; NAMPT, Nicotinamide phosphoribosyltransferase; KSP, kinesin spindle protein; CENP-E, Centrosome-associated protein E; SRC (a nonreceptor protein tyrosine kinase); NAE, NEDD8-activating enzyme; PLK1, polo-like kinase 1; CRM1, chromosomal maintenance 1; PCK, protein kinase C; PDK, phospholipid-dependent kinase; CHK, checkpoint kinase; CDK2, cyclin-dependent kinase 2.

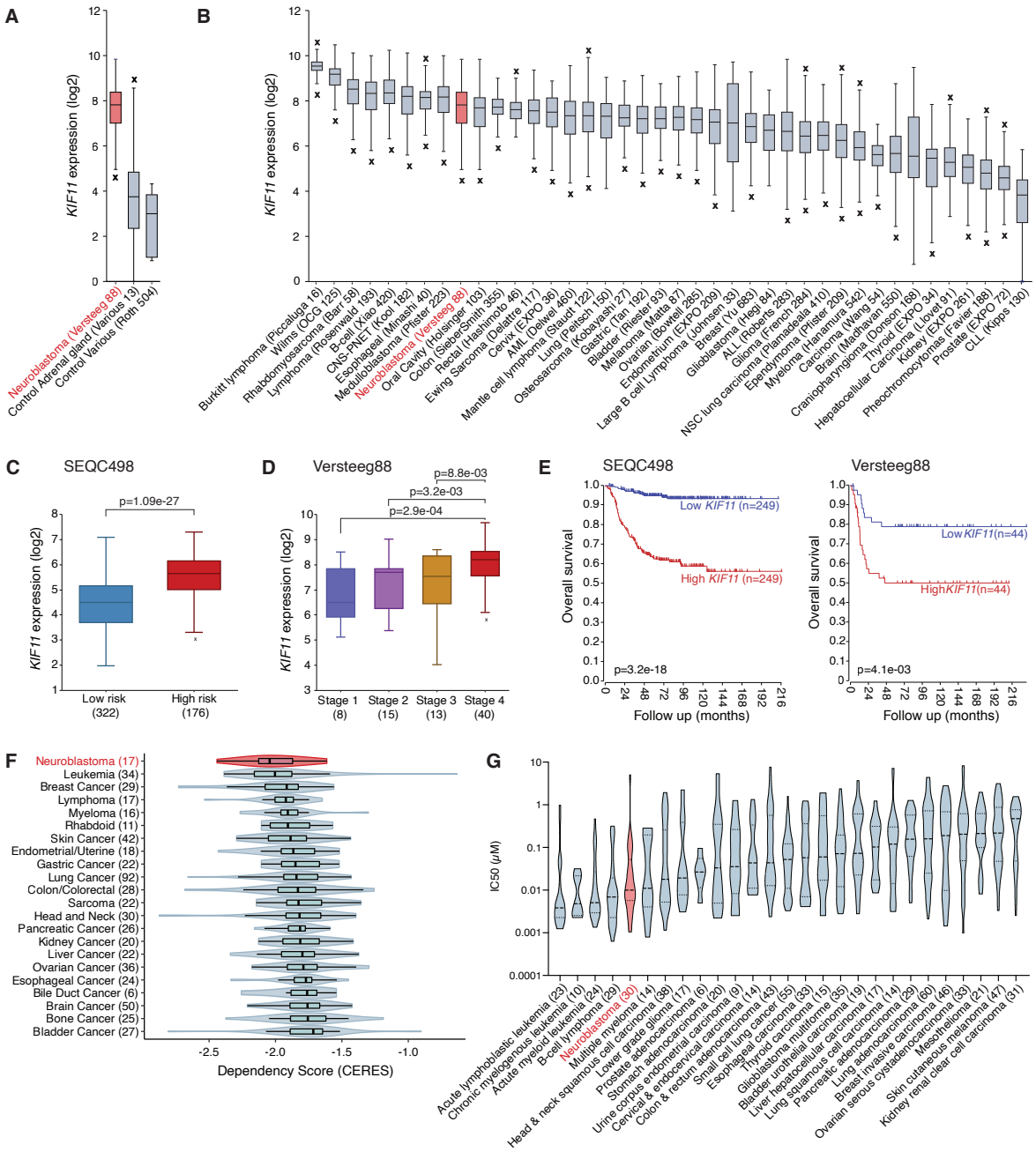

Figure 3. *KIF11* gene expression, dependency, and responsiveness to ARRY-520 in neuroblastoma. (A) *KIF11* expression in neuroblastoma patient samples compared to that in normal control tissue samples. Data for control adrenal gland are presented separately from other control tissues. **(B)** *KIF11* expression across 40 tumor types. **(C)** *KIF11* expression in low-risk and high-risk neuroblastoma patient tumors within the SEQC498 patient cohort. Statistical analysis was performed using the two-sided unpaired t-test. **(D)** *KIF11* expression in patient tumor samples from the Versteeg88 patient cohort, grouped based on INSS stage 1-4.

Statistical analyses were performed using the two-sided unpaired t-test. **(E)** Survival of neuroblastoma patients with high and low *KIF11* gene expression (median used as cutoff) in the SEQC498 and Versteeg88 datasets presented using Kaplan-Meier survival curves. Statistical analyses were performed using the log-rank test. In panels A – E, data are from publicly available patient cohorts (R2: microarray analysis and visualization platform) and were visualized with R2. Box plots show upper and lower quartile and whiskers represent minimum and maximum. **(F)** *KIF11* gene dependency across 22 tumor types presented using the CERES dependency score based on CRISPR-Cas9–based viability screens from a publicly available dataset (DepMap portal). A low score indicates high gene dependency. **(G)** Sensitivity to ARRY-520 treatment across 27 different tumor types. Analysis of data from the Genomics of Drug Sensitivity in Cancer (GDSC) screening program. Data are presented as IC_{50} (μM). INSS, International Neuroblastoma Staging System; KSP, kinesin spindle protein.

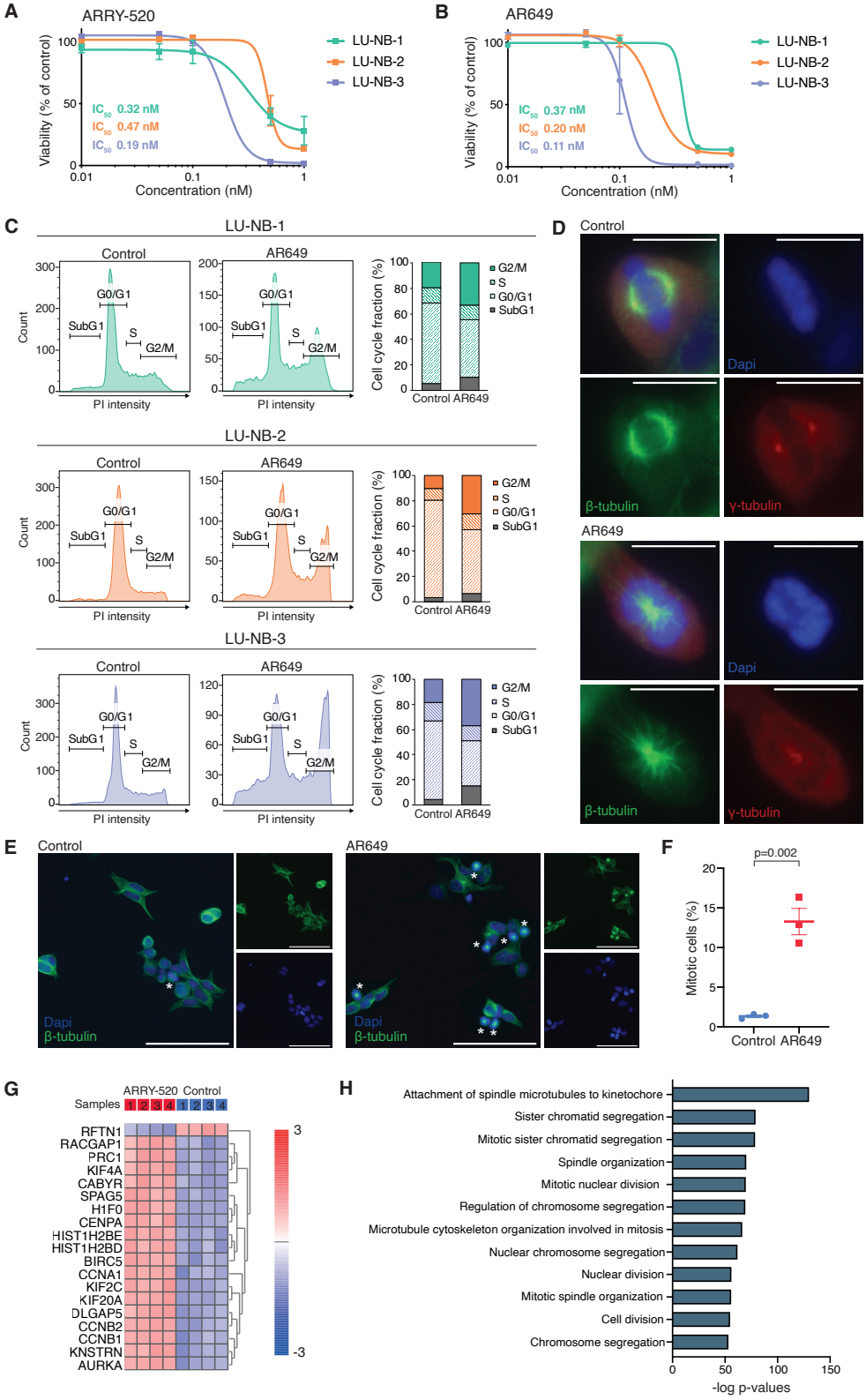

Figure 4. KSP inhibition causes mitotic arrest and formation of monopolar spindles. LU-NB-1, LU-NB-2, and LU-NB-3 PDX cells were treated with KSP inhibitors (ARRY-520 or AR649) at the indicated concentrations prior to analysis. **(A-B)** Cell viability after 72 h for

ARRY-520 or AR649 treatment as measured using CellTiter-Glo. Values are shown as mean percent viability of control ± SEM from three independent experiments. Control cells were treated with DMSO. **(C)** Flow cytometry analysis of cell cycle progression of the neuroblastoma cells following AR649 treatment (0.5 nM, 24h). Bar graphs show representative data from two independent experiments. **(D)** Immunofluorescence of LU-NB-2 PDX cells treated with AR649 (0.5 nM, 24h) and stained with β-tubulin (green), γ-tubulin (red), and DAPI (blue). Scale bars represent 10 µm. **(E)** Representative photographs of LU-NB-2 cells stained with β-tubulin (green) and DAPI (blue). Asterisks indicate mitotic cells. Scale bars represent 100 µm. **(F)** Quantification of mitotic LU-NB-2 PDX cells following AR649 treatment (0.5 nM, 24h). Data from three independent experiments are shown, error bars show SEM, and statistical analysis was performed using the two-sided unpaired t-test. **(G)** Transcriptomic analysis of the LU-NB-2 PDX cell response following ARRY-520 treatment. Cells were treated in quadruplicates with 0.5 nM ARRY-520 for 24 h and analyzed by RNA sequencing. Heat map shows the differentially expressed genes between treatment group and controls as identified by ANOVA ($p < 0.01$, FDR correction). **(H)** Gene ontology analysis of genes with higher expression in ARRY-520–treated samples from (G).

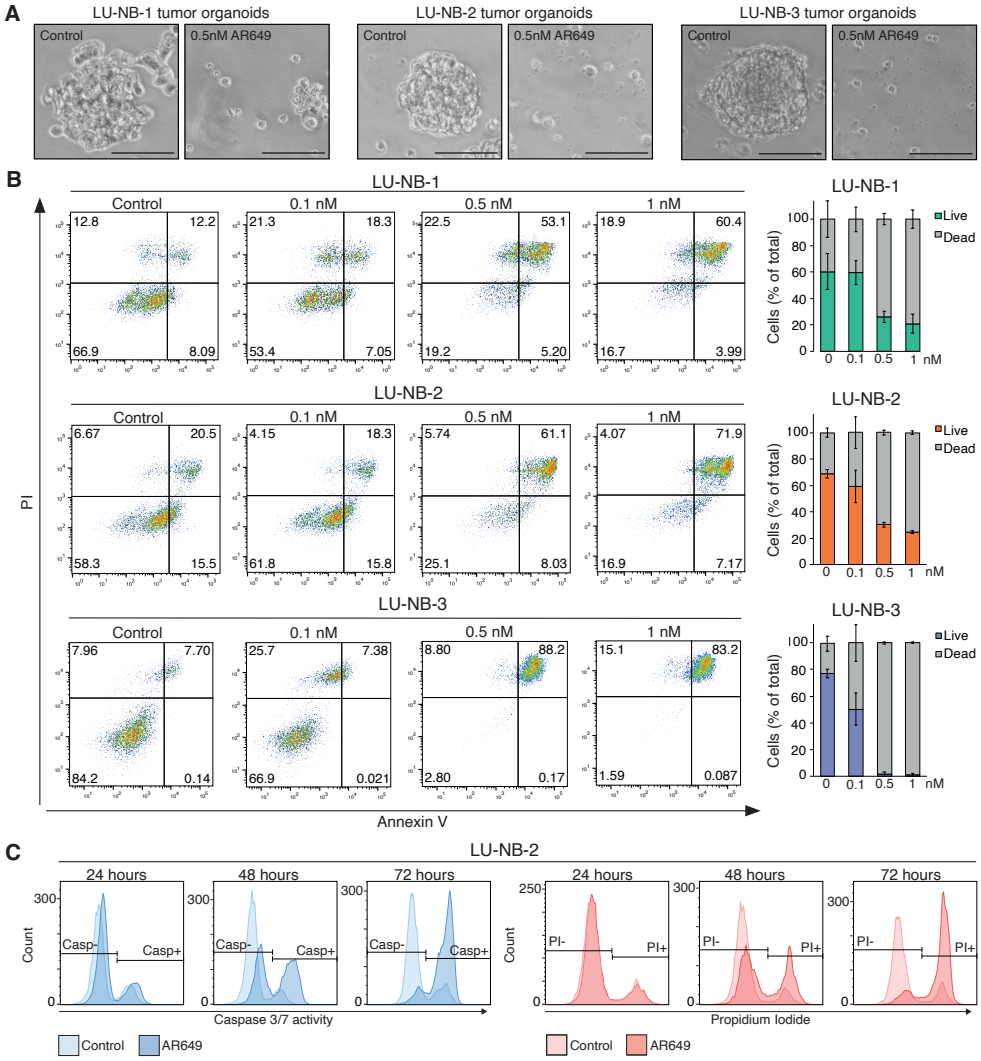

Figure 5. KSP inhibition results in neuroblastoma cell death. **(A)** Representative photographs of neuroblastoma organoids treated with AR649 (0.5 nM for 72 h). Scale bars represent 200 µm. **(B)** Annexin V and propidium iodide (PI) flow cytometry analysis of cell death following AR649 treatment at increasing concentrations. Bar graphs show quantification of live and dead cells; Live cells = PI negative; dead cells = PI positive. Bars show mean values ± SEM from three independent experiments. **(C)** LU-NB-2 PDX cells were treated with 0.5 nM AR649 at three time points (24, 48, and 72 h) and analyzed for caspase-3/7 activity (apoptotic cells) and by PI staining (dead cells). Caspase activity was detected using NucView405.

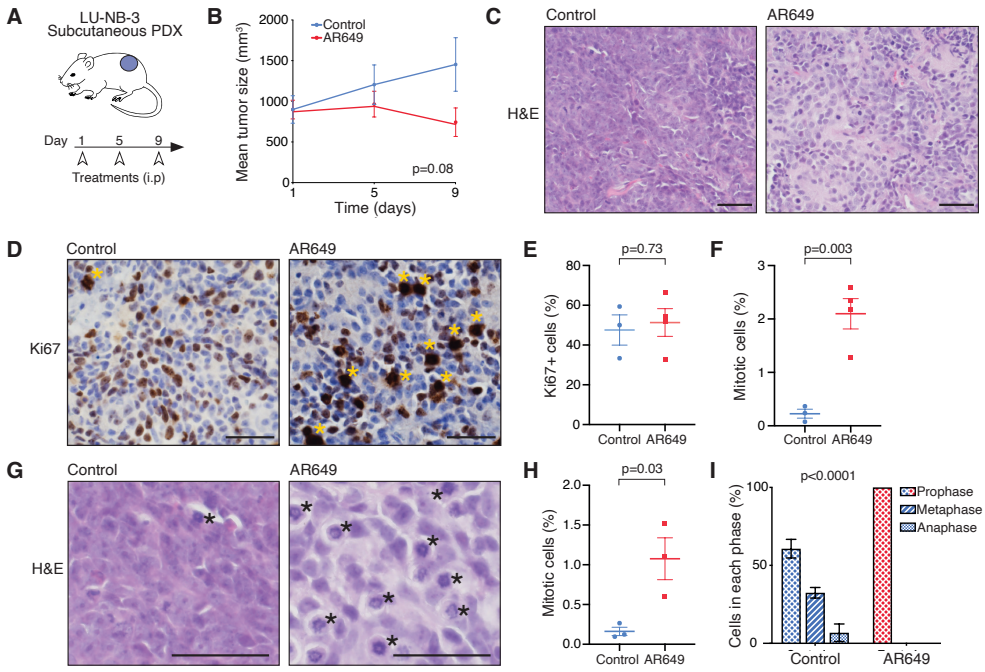

Figure 6. KSP inhibition causes differentiation and mitotic arrest in vivo. (A) Short-term treatment of LU-NB-3 PDX tumors in nude mice. LU-NB-3 cells were subcutaneously injected into nude mice. When tumors reached 500 mm^3, mice were treated with AR649 (5 mg/kg, intraperitoneal injection (i.p), n=5) or saline (n=4) on day 1, 5, and 9, and then euthanized. **(B)** Tumor size (mean ± SEM) of treated tumors measured using digital caliper. Statistical analysis was performed using the two-sided unpaired t-test. **(C)** Hematoxylin & eosin (H&E) staining of PDX tumor sections. **(D)** Ki67 staining of tumor sections. Asterisks indicate mitotic cells. **(E-F)** Quantification of $Ki67^+$ cells and mitotic cells identified from Ki67 staining compared to the total number of cells on each slide. Symbols represent mean of three slides from one tumor, error bars show SEM, and statistical analysis was performed using the two-sided unpaired t-test. **(G)** H&E staining of PDX tumor sections. Asterisks indicate mitotic cells. **(H)** Quantification of mitotic cells from H&E staining compared to the total number of cells in each slide. Symbols represent mean of three slides from one tumor, error bars show SEM, and statistical analysis was performed using the two-sided unpaired t-test. **(I)** Quantification of the distribution of mitotic cells in prophase, metaphase, or anaphase in H&E stained tumors. Data

from three tumors per group are shown, error bars show SEM, and statistical analysis was performed using the two-tailed Mann-Whitney U test. Scale bars represent 40 µm.

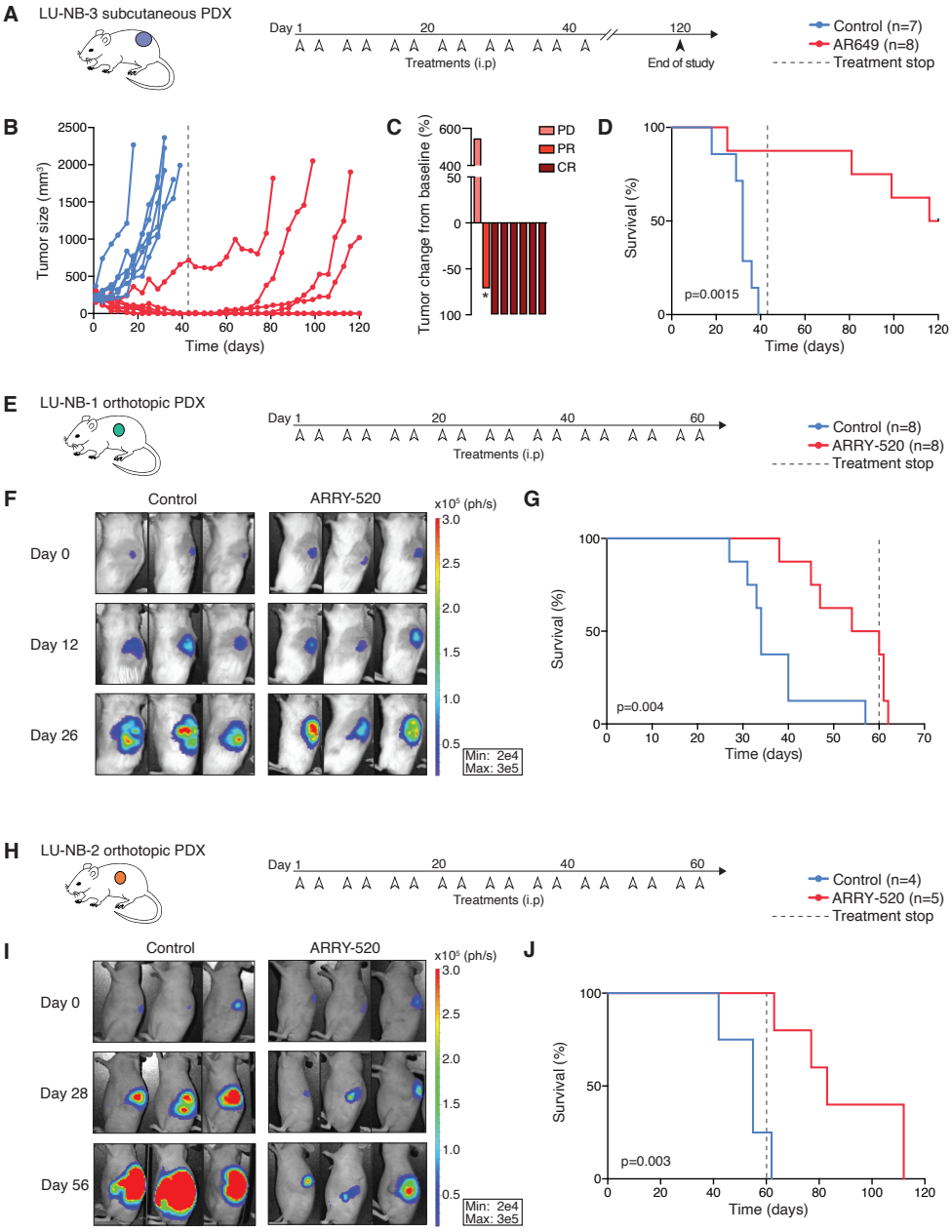

Figure 7. KSP inhibition prolongs survival of mice with neuroblastoma orthotopic PDX tumors. (A) PDX model and treatment regimen. Neuroblastoma LU-NB-3 PDX tumors were established following subcutaneous injection in nude mice. Mice were treated i.p. with AR649 (1.5 mg/kg, n=8) or saline (n=7) in vivo twice a week for six weeks. **(B)** Tumor volume for each mouse from first treatment day, measured using digital caliper. Mice were euthanized

when tumor size reached ≥1800 mm^3 **(C)** Response of each mouse in the AR649 treatment group on the last treatment day (day 42). Asterisk indicates mouse euthanized due to weight loss. Responses were classified as complete response (CR) if tumors regressed 100%, partial response (PR) if tumor regression was less than 100%, and progressive disease (PD) if tumors grew. **(D)** Kaplan-Meier curves show the survival in days from first treatment day of LU-NB-3 PDX mice following AR649 treatment. Statistical analysis was performed using the log-rank test. **(E)** PDX model and treatment regimen. Orthotopic neuroblastoma LU-NB-1 PDX tumors were established in NSG mice, and mice were treated i.p. with ARRY-520 (12.5 mg/kg, n=8) or saline (n=8) twice a week for nine weeks. **(F)** Representative bioluminescence imaging in vivo, see fig. S12C for all mice. **(G)** Kaplan-Meier curves show the survival in days from first treatment day of LU-NB-1 orthotopic PDX mice following treatment. Statistical analysis was performed using the log-rank test. **(H)** PDX model and treatment regimen. Orthotopic neuroblastoma LU-NB-2 PDX tumors were established in nude mice, and mice were treated i.p. with ARRY-520 (12.5 mg/kg, i.p., n=5) or saline (n=4) twice a week for nine weeks. **(I)** Representative bioluminescence imaging in vivo, see fig. S13C for all mice. **(J)** Kaplan-Meier curves show the survival in days from first treatment day of mice following ARRY-520 treatment of LU-NB-2 orthotopic PDX models. Statistical analysis was performed using the log-rank test. i.p., intraperitoneal injection.